Available online at www.sciencedirect.com
ScienceDirect
Surface Science 601 (2007) 498–509
SURFACE SCIENCE
www.elsevier.com/locate/susc

Observation and investigation of graphite superlattice boundaries by scanning tunneling microscopy

Wing-Tat Pong, James Bendall, Colm Durkan *

Nanoscience Centre, University of Cambridge, 11. J.J. Thomson Avenue, Cambridge, CB3 0FF, UK

Received 21 June 2006; accepted for publication 10 October 2006
Available online 3 November 2006

Abstract

In this article, we report on scanning tunneling microscopy (STM) observations of several different kinds of superlattice boundaries on highly-oriented pyrolytic graphite (HOPG) including an array of bead-like structures, a monolayer deep trench, a zig-zag shaped termination, and a plain boundary without features. Results of a simulation model show that a top rotated graphite layer with a straight boundary does not necessarily lead to the zig-zag shaped boundary of the resulting superlattice as has been previously claimed. The formation of the bead-like, trench, and zig-zag shaped boundaries is explained from the energetic point of view. Our study also shows evidence for the superlattice-mediated observation of a low-angle grain boundary with a varying tilt angle. A relationship between the periodicity of the boundary dislocations and the periodicity of the superlattice across the boundary is derived. The result of this work is important for an understanding of superlattices on graphite whose origin is not yet completely understood.

Keywords: Scanning tunneling microscopy; Surface electronic phenomena; Surface structure; Morphology; Roughness; Topography

1. Introduction

Although superlattices on graphite have been observed many times by scanning tunnelling microscopy (STM) [1–13], a complete understanding has yet to be achieved as to their physical origins. Several theories and hypotheses ranging from Moiré interference patterns due to a mis-orientation of two layers of graphite, to sub-surface arrays of nanoscale defects have been proposed to explain the origin of superlattices [1,4,14,15]. To date however, not much discussion has been focussed on superlattice boundaries, which is an intriguing subject on its own due to the fact that the boundary is the region where the transition from normal graphite to a superlattice occurs. In this article, we report on our observations of several different types of superlattice boundaries by STM.

* Corresponding author. Tel.: +44 1223 760301; fax: +44 1223 760309.
E-mail address: cd229@eng.cam.ac.uk (C. Durkan).

0039-6028/$ - see front matter © 2006 Elsevier B.V. All rights reserved.
doi:10.1016/j.susc.2006.10.012

2. Experimental protocol

Highly oriented pyrolytic graphite (HOPG) with 0.4° mosaic spread was freshly cleaved with either a scalper or scotch tape before being imaged with a home-built STM [16] or a Nanosurf STM [17] in constant current mode under ambient conditions. Mechanically cut Pt/Ir tips were used.

3. Observations of superlattice boundaries

In this section we will briefly describe each of the different types of superlattice boundary we have observed. An in-depth discussion and analysis follows in Section 4.

3.1. Array of bead-like structures (Fig. 1)

At the intersection between the normal graphite (i.e. a superlattice-free region) and a superlattice (which, in this case has a periodicity of 6.5 nm) there is an uneven

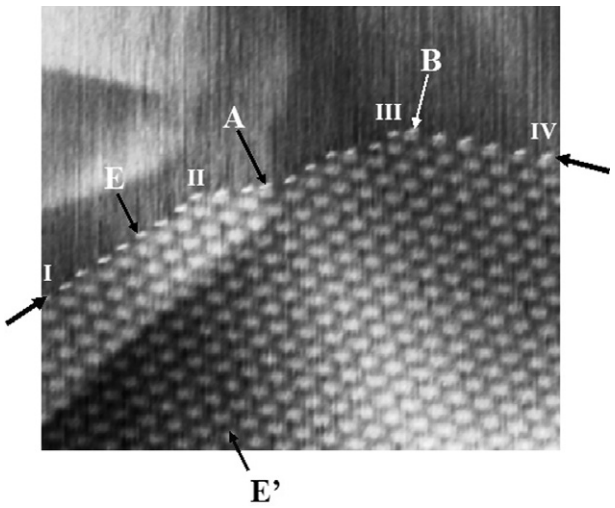

Fig. 1. 106 nm × 123 nm image, $I_t = 0.5$ nA, $V_t = 230$ mV, periodicity of the superlattice = 6.5 nm. The array of bead-like structure, which is the boundary for the superlattice, is indicated by the thicker arrows. At locations A and B, the bead-like boundary cuts through the bright spots of the superlattice which are of higher energy. If we look at the superlattice row by row each along the direction EE′, each bead on the boundary corresponds to each row of the superlattice.

boundary (sections I–II and III–IV of the boundary are relatively straight and parallel with the superlattice whereas section II–III is uneven and not parallel with the superlattice) along which there is an array of bead-like structures whose corrugation is 0.26 nm, larger than the superlattice corrugation of 0.17 nm. Observations of similar boundary structures have previously been reported in the literature [1,4,15,18]. Traversing the boundary indicated by the thick arrows in Fig. 1, the position of each bead on the boundary corresponds to each row of the superlattice (along the direction EE′). The boundary intersects localised regions of increased electron density of the superlattice (which appear as bright spots (''beads'') in the image), for example at locations A and B. According to the tight-binding density calculation of the electronic states on graphite by Charlier et al. [19], these bright spots are of AAB stacking [5] with higher energy of 0.0085 states/eV than the surrounding regions. It appears that the exact location and orientation of the superlattice boundary determines the boundary's appearance.

3.2. One monolayer deep trench (Fig. 2)

The superlattice is terminated by a trench which appears to be one monolayer deep. The surface heights on each side of the trench are equal. The trench is oriented parallel to the superlattice rows and stretches through the lower points of the superlattice without dissecting the bright spots. According to the calculation of Charlier et al. [19], the lower valleys of superlattices are of ABC stacking with lower energy of 0.0021 states/eV [5], thus such a boundary should be energetically stable as it does not involve the disruption of the high energy superlattice peaks.

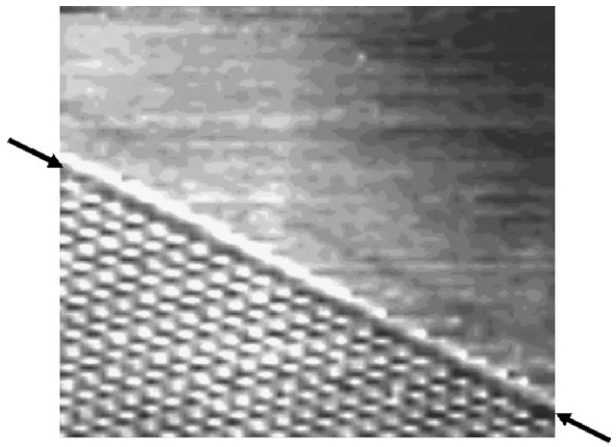

Fig. 2. 127 nm × 145 nm, $I_t = 0.5$ nA, $V_s = 206$ mV, periodicity of the superlattice = 5.0 nm. The trench, indicated by the arrows, has depth of approximately 0.33 nm.

3.3. Zig-zag shaped boundary (Fig. 3)

The superlattice is terminated by a monatomic step with a zig-zag shape. This kind of zig-zag shaped boundary has been observed previously [2,11]. In all of these results, the zig-zag shaped boundaries appear to go around the superlattice bright spots rather than through them.

3.4. Plain boundary without features (Fig. 4b)

The intersection is a plain boundary without features (Fig. 4b). Unlike the trench or the zig-zag shaped boundaries, it dissects some of the superlattice bright spots. On the left of the superlattice lies a double-stranded ribbon-like structure (G_2B_2) with a width of approximately 3.5 nm and height of 0.3 nm (Fig. 4c). It has a corrugation of 0.2 nm and periodicity of 1.3 nm. Apparently the ribbon-like structures G_2B_2 and G_1B_1 (see Fig. 4a) were

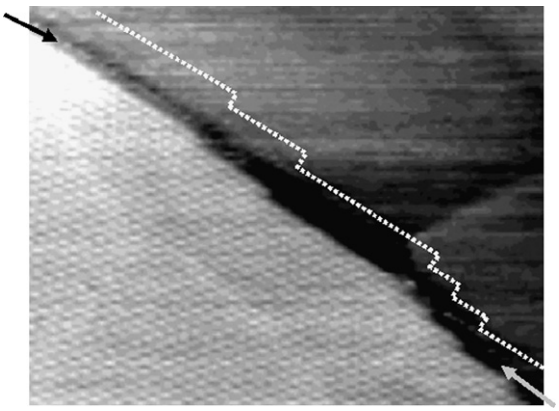

Fig. 3. 200 nm × 254 nm, $I_t = 0.5$ nA, $V_s = 206$ mV, periodicity of the superlattice = 5.3 nm. The zig-zag shaped termination is pointed by the arrows. Dashed line for guiding eyes on the zig-zag shape of the boundary.

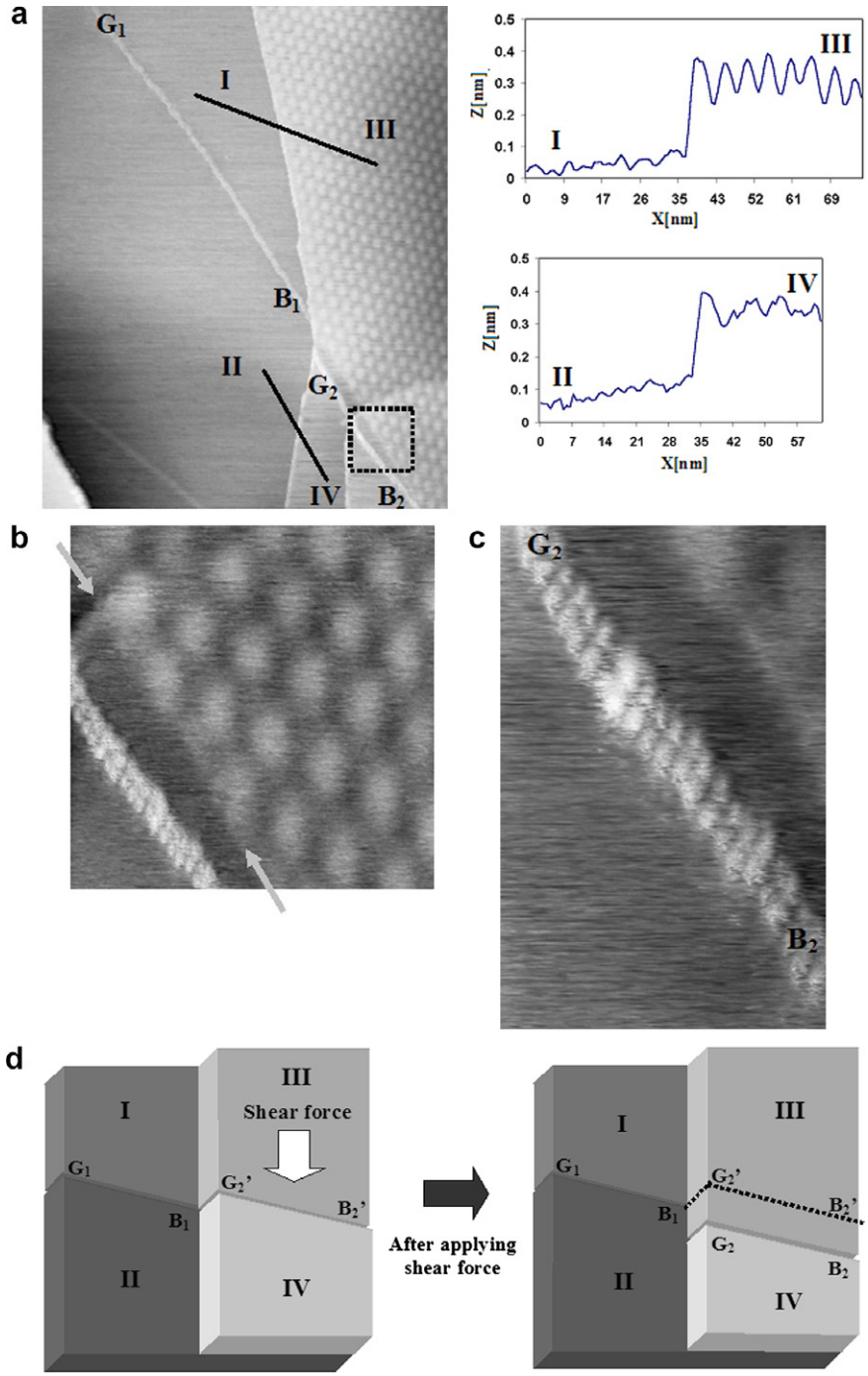

Fig. 4. (a) 157 nm × 194 nm, $I_t = 0.5$ nA, $V_t = 230$ mV. This image shows the location of the plain boundary and the grain boundaries associated with it. The cross-sections show that regions III and IV are one monolayer higher than regions I and II. (b) The zoom-in of the framed area in Fig. 5a. 39 nm × 39 nm, $I_t = 0.5$ nA, $V_t = 230$ mV, periodicity of the superlattice = 7.1 nm. The plain boundary (pointed by the arrows), unlike the other kinds of boundaries, does not have any particular features. (c) 17.6 nm × 27.6 nm, $I_t = 0.5$ nA, $V_t = 230$ mV. A zoom-in of the double-stranded ribbon-like structure on the left of the plain boundary. It shows the periodic feature on the ribbon. (d) A model explaining the relative movement of the graphene sheets next to the grain boundary.

originally the same ribbon, but they are shifted away from each other with the offset coincidently being the same as the separation between the plain boundary and the G_2B_2. Similar features have been observed before with width from 10 to 16 nm, height from 1 to 3 nm, and more than 6 μm in length, which are about 10 times larger than the one reported here [20]. It was proposed that this is representative of a disrupted graphite surface and may be associated with flaking of the surface [20]. Other groups have observed similar strand-like structures with ordered features [7,9,21]. Gan et al. regarded this kind of double-stranded ribbon-like structure as a grain boundary [22].

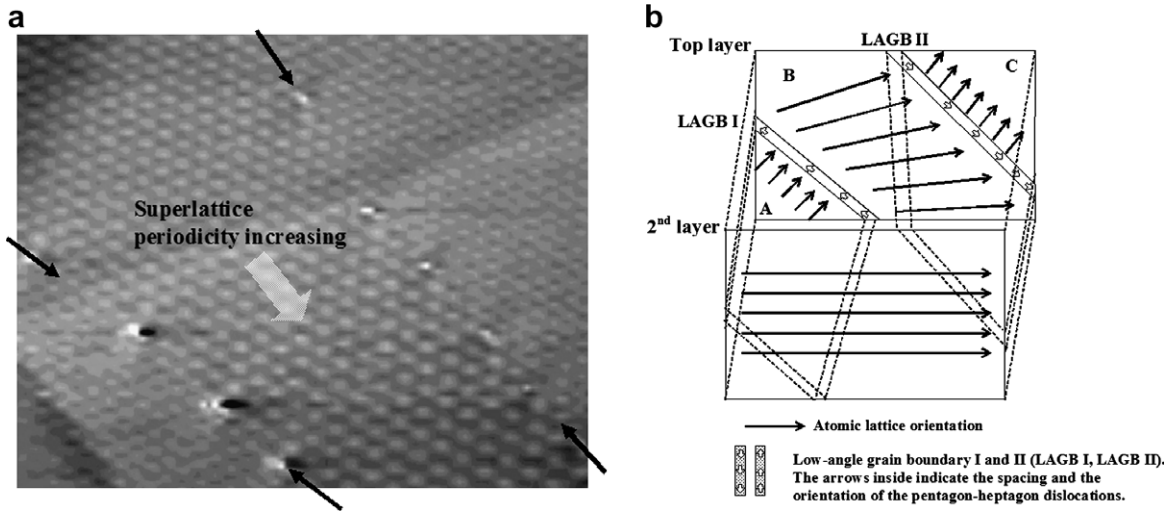

Fig. 5. (a) 162 nm × 204 nm, $I_t = 0.5$ nA, $V_s = 206$ mV, the superlattice periodicity varies from around 9.6 to 7.1 nm within the boundaries which are in the form of the arrays of protrusions. The boundaries with arrays of protrusions are indicated by the black arrows. (b) Schematic model explaining the formation of the conventional superlattices outside the superlattice region with varying periodicities. The low-angle grain boundary LAGB I converts the conventional superlattice region A into superlattice B with varying periodicity while LAGB II converts it back to conventional superlattice region C. The effects of the LAGBs on the atomic lattice orientation are illustrated in the figure.

Comparing the ribbon-like structure G_2B_2 in Fig. 4c with GB in Fig. 1d in Ref. [22], both of them have periodic features and their periodicities and corrugations are of similar order of magnitude, therefore it is likely G_1B_1 and G_2B_2 in Fig. 4a and c are also grain boundaries as the GB in Ref. [22].

3.5. Array of protrusions with uneven spacing (Fig. 5)

Here we observe a superlattice region with varying periodicity (from 7.1 to 9.6 nm) between the two conventional superlattice regions, and the intersection which marks the boundary is an array of protrusions with uneven spacing of tens of nanometres. Those protrusions have a range of heights from 0.34 nm at the lower side to 0.52 nm at the upper side. A superlattice region with varying periodicity was observed by Bernhardt et al. [7], but in that case, the superlattice was in a pit and so the boundary is a step edge.

4. Discussion

We have performed investigations into these superlattice boundaries from the energetic point of view. First, we will study the zig-zag shaped boundary. The zig-zag shaped boundary was discussed before and it was speculatively proposed that when the top graphite layer has a straight boundary, the observed superstructure which is induced by Moiré-type interference between the electronic wave-functions in adjacent grapheme layers must have a zig-zag shape at the boundary [11,23]. We have analyzed the zig-zag shaped boundary with a simulation model which can simulate graphite layers by using Eq. (1) [24]:

$$\Phi_n = 1 - \frac{2}{9}\left[\cos\left[\left(\frac{2\pi}{2.46}\right)\left(x'' + \frac{y''}{\sqrt{3}}\right)\right] + \cos\left[\left(\frac{2\pi}{2.46}\right)\left(x'' - \frac{y''}{\sqrt{3}}\right)\right] + \cos\left[\left(\frac{4\pi}{2.46}\right)\left(\frac{y''}{\sqrt{3}}\right)\right] + \frac{3}{2}\right], \quad (1)$$

where Φ_n is the atomic density of layer n at a position (x, y), x'' and y'' are the modified coordinates (x, y) after taking into account the rotation of a graphite layer (refer to Eqs. (8) and (9) in Ref. [25]) and the relative shifting between alternate graphite layers (refer to Eqs. (6) and (7) in Ref. [25]). The details of this simulation model can be found in Ref. [25]. A Moiré rotation-induced superlattice can be simulated with this model. Fig. 6 shows a graphite model with a superlattice in the shape of a parallelogram. This model is built up with the top layer in the form of a parallelogram stripe, overlaid on a second layer, as schematically shown in Fig. 6a. There is a misorientation angle between the atomic lattices of the top layer and the second layer. According to Refs. [11,23], when the top rotated layer has a straight boundary, we should observe a zig-zag shaped boundary with STM. In fact, we find experimentally that depending on its direction, the superlattice boundary does not necessarily have to intersect the bright spots. It can extend through the lower points (dark spots, or regions of reduced electron density) of the superlattice, and therefore does not result in a zig-zag shape as suggested. This argument is supported by our simulation results. We have simulated the superlattice which arises when the top graphite layer in the form of a parallelogram stripe (length = 30 nm, width = 16.5 nm, area = length × width = 495 nm^2) has its atomic lattice rotated by 8° (θ) with respect to the second layer (length = 30 nm, width = 30 nm), and where the boundary of the top layer

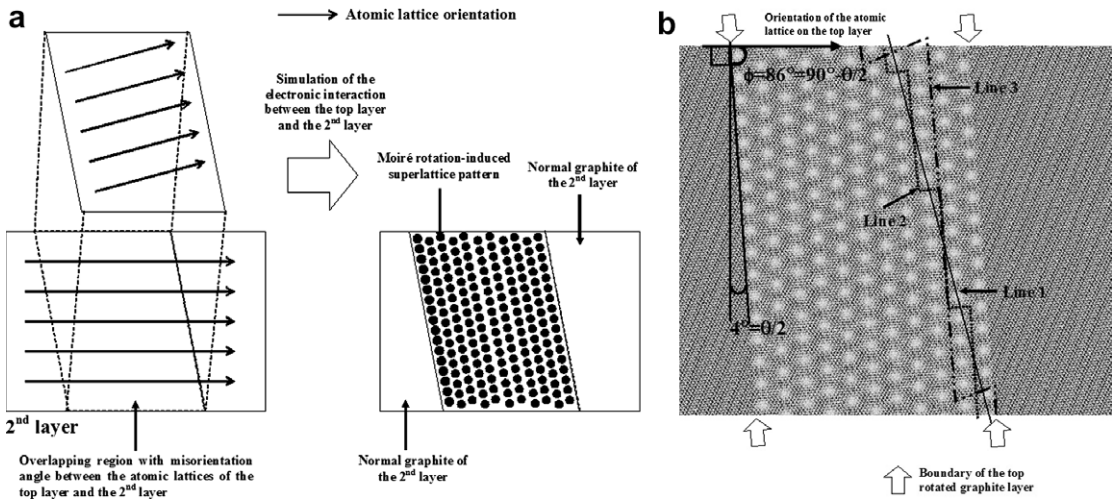

Fig. 6. 30 nm × 30 nm simulated graphite area with the top layer as a stripe in the shape of a parallelogram with the length of 30 nm and width of 16.5 nm, giving an area of 495 nm^2, whose atomic lattice is rotated 8° (θ) with respect to the second layer with the size of 30 nm × 30 nm. The top rotated layer has straight boundaries which are the same boundaries as the resulting superlattice. (a) Schematic model of the simulation. The top layer is a parallelogram stripe and the second layer is rectangular in shape; there is a misorientation angle between their atomic lattices as shown by the atomic lattice orientations in the figure. After simulating the electronic interaction between the two layers, Moiré superlattice pattern is formed on the overlapping region. (b) The simulation is performed with normal weightings of 0.5 for the first layer and 0.125 for the second layer. The configuration of the weightings of each layer for simulation of graphite is described and explained in Refs. [6,15,25]. The simulation results shows a superlattice with a straight boundary rather than zig-zag shaped boundary which is expected by the theory proposed in [11 and 13].

is straight with an angle of 4° ($\theta/2$) with respect to the perpendicular direction (see Fig. 6). Although it has a straight termination for its top layer, the simulation result shows that the resulting superlattice boundary does not intersect the bright spots, and thus would not form the zig-zag shape boundary according to the mechanism in Refs. [11,23]. Moreover, as the boundary just cuts through the lower valleys which are of ABC stacking with lower energy (0.0021 states/eV) [5], it is energetically more stable. Hence a top rotated graphite layer with a straight termination can still form a superlattice with a straight boundary.

We would like to propose a physical reason for the origin of the zig-zag shaped boundary which was not reported before. Rong and Kuiper [1] show that the orientation angle of a Moiré superlattice pattern with respect to the top graphite layer is given by

$$\phi = 30^\circ - \theta/2, \tag{2}$$

where θ is the rotation between the graphite layers which causes the superlattice, as is schematically shown in Fig. 7. As we can see from the model, there are certain distinct angles where the boundary is parallel to an axis of the superlattice: $\phi = 30^\circ - \theta/2$, $\phi = 60^\circ - \theta/2$, $\phi = 90^\circ - \theta/2$, $\phi = 120^\circ - \theta/2$, $\phi = 150^\circ - \theta/2$, $\phi = 180^\circ - \theta/2$ (the superlattice simulated in Fig. 6 has an angle of $\phi = 90^\circ - \theta/2$). The probability of having the top rotated layer boundary exactly along one of these directions is rather small and the more likely situation is that the boundary intersects the bright spots as shown by line 1 in Fig. 6b. However, the bright spots are of AAB stacking whose energy is higher (0.0085 states/eV), and thus the boundary along line 1 is not energetically favourable. Instead of line 1, the top layer boundary has a tendency to select line 2 because this line only cuts through energetically low points and is thus more stable. Line 2 is preferred to line 3 because it takes less effort to change from line 1 to line 2 as line 2 is the most similar to line 1. In light of this, the boundary of a top rotated layer has a tendency of avoiding intersecting superlattice bright spots due to the consideration of energy. Instead, a boundary inclines to go around superlattice bright spots so as to achieve an energetically more stable situation, resulting in a zig-zag shape. Since the top rotated layer has a zig-zag shape, the resulting Moiré superlattice will have a zig-zag shape as well. The situation is illustrated by the simulation. A superlattice simulation similar to the one in Fig. 6 where the top layer is in the form of a parallelogram and the second layer is in the form of a rectangle is carried out and shown in Fig. 8. However, in this simulation, the right-hand edge of the top layer which is originally straight as in Fig. 6 is replaced by line 2 which is zig-zag in shape as shown schematically in Fig. 8a. The simulation result in Fig. 8b shows a superlattice with the zig-zag shaped boundary as line 2 which indicates that a superlattice with a zig-zag shaped boundary is possible if the boundary of the rotated layer itself is zig-zag in shape which is the case when the straight edge of the top rotated layer is not parallel with the axis of the superlattice as discussed above. The zig-zag shaped boundary of the simulated superlattice in Fig. 8b is similar to the zig-zag shaped boundary in Fig. 3, except their periodicities of the transition edges are different. We conclude that a possible reason why a zig-zag shaped boundary occurs is as it is a way to lower the boundary energy.

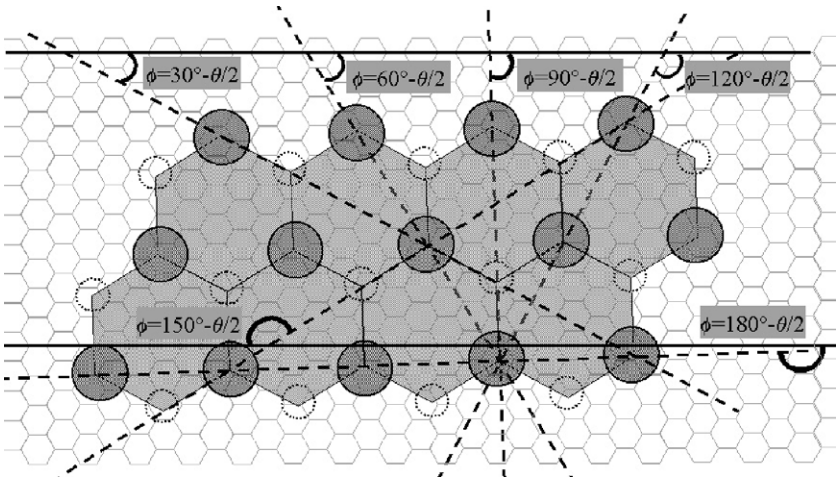

Fig. 7. This model illustrates the orientation angle of the superlattice with respect to the top graphite layer. The smaller hexagonal lattices underneath are the top graphite layer while the big closed circles are the brightest spots of the superlattice; the small open circles outlined with dashed lines are the medium bright spots of the superlattice. The orientation of the Moiré superlattice pattern is $\phi = 30° - \theta/2$ relative to the top graphite layer with θ being the rotation angle between the top two graphite layers which causes the superlattice. We can see that in order to go in parallel with a superlattice, the boundary has to be with one of the angles ϕ indicated in the figure.

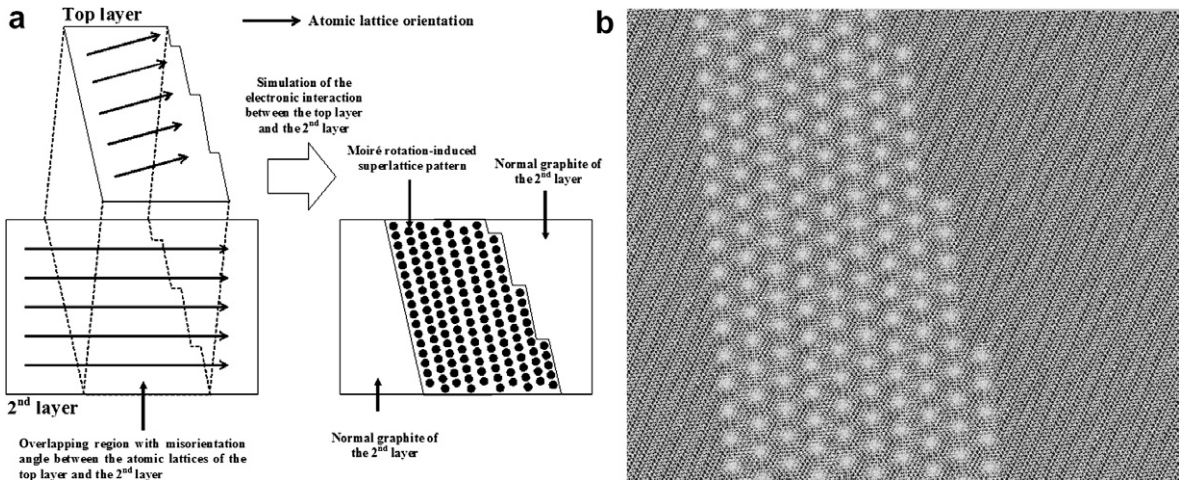

Fig. 8. The same simulation model as in Fig. 6 with the same rotation angle of 8°, weightings and size of area, but the boundary for the top rotated layer is along line 2 in Fig. 6. (a) Schematic model of the simulation. The top layer is also a parallelogram stripe as in Fig. 6a but its right edge is zig-zag shaped. The second layer is the same as in Fig. 6a, which is a rectangle. There is a misorientation angle between their atomic lattices. After simulating the electronic interaction between the two layers, Moiré superlattice pattern is formed on the overlapping region. (b) As we can see here from the simulation result, the boundary of the superlattice is the same as that of the top layer, which is zig-zag in shape.

In short, when a Moiré superlattice pattern is formed by a top graphite layer with an edge, either kind of the superlattice boundaries may occur: (a) if the straight edge of the top layer is parallel to the axis of the superlattice and does not intersect the superlattice bright spots, the resulting superlattice boundary will have the same straight edge as the top layer; (b) if the edge of the top layer attempts to intersect the superlattice bright spots which is the case when the edge of the top layer is not parallel to the axis of the superlattice, the edge of the top layer will tend to go around the superlattice bright spots and thus it will be zig-zag in shape, resulting in the zig-zag shaped boundary of the Moiré superlattice pattern.

Now consider the case where our line labelled "1" happens to be the boundary and the edge of the top layer intersects the superlattice bright spots despite the consequence that it will result in higher energy. Since the superlattice bright spots are of high energy, when the boundary intersects them, the high energy points are terminated sharply and form some sites of concentrated electronic density. As the STM is probing the density of states at the Fermi level, these points consequently appear brighter than the other high points of the superlattice. This explains the bead-like boundary in Fig. 1 and the correspondence between each bead and each superlattice row. Although sections I–II and III–IV of the boundary in Fig. 1 are

parallel to the axis of the superlattice, they are intersecting the superlattice bright spots and thus the boundary appears as bead-like structures in these sections as well.

Using similar arguments, the trench boundary in Fig. 2 is oriented parallel to an axis of the superlattice and does not cut through those high energy bright peaks, therefore the boundary is straight without an array of bead-like structures, as discussed earlier. The appearance of a monolayer deep trench between the superlattice and the boundary is simply due to the position of the boundary, and is not in fact an actual physical trench. From the image, it is found that the peak–peak amplitude of the superlattice is around 0.4 nm, and the boundary happens to lie along the row of dips of the superlattice, thus it appears as a trench in the STM image.

The situation of the plain boundary in Fig. 4b is more complicated as it does intersect the superlattice bright peaks, yet no bead-like structures are apparent. The coincidence of the matching of the offset between G_1B_1 and G_2B_2 with the spacing between the plain boundary and G_2B_2 is related to the origin of the plain boundary. As mentioned before, G_1B_1 and $G_2'B_2'$ ($G_2'B_2'$ is the original position of G_2B_2 before the shear force is applied) were originally the same grain boundary, but possibly due to some shear force, there was a slip between the two graphite layers which caused the offset between G_1B_1 and G_2B_2 (see Fig. 4d). The situation in Fig. 4a is schematically shown in the model of Fig. 4d where regions III and IV are one monolayer higher than regions I and II as displayed in the cross-sections of Fig. 4a of I–III and II–IV. The misorientation between region I and region III induces the Moiré rotation pattern which we observe as a superlattice structure. Region III extends into a part of region II and it happens that there is no misorientation between region II and region III, therefore no superlattice appears in the region between G_2B_2 and $G_2'B_2'$. Since the boundary of region I is along $G_2'B_2'$, the transition from the superlattice to the normal graphite occurs along the direction of $G_2'B_2'$on the second layer, rather than on the topmost layer. As the bisection of the bright peaks occurs underneath the surface, it is no surprise that no sites of concentrated electronic density (bead-like structures) are observed on the topmost layer under the STM. Ouseph [13] used a similar model with a slip of a section of the graphite layer on one side of the dislocation ribbon with respect to the section of the layer on the other side to explain the formation of the superlattice successfully.

The boundary in Fig. 5 consists of a line of protrusions with a spacing of tens of nanometres, where the spacing of these protrusions increases from the bottom to top while the superlattice periodicity within the boundaries increases from the top to bottom. It appears that each "protrusion" is in fact a dislocation, and the array of dislocations is consistent with the dislocation network for a low-angle grain boundary [26]. The differences in the superlattice periodicities across the boundaries are related to the tilting between the graphite lattices on the two sides of the boundaries. The difference in superlattice periodicities can be interpreted as the difference in the rotation angles of the graphite layers across the boundary since the rotation angle θ is related to the superlattice periodicity P_S (in nm) by Eq. (3):

$$\theta = 2\sin^{-1}\left(\frac{0.246}{2P_S}\right). \tag{3}$$

The tilt angle at the low-angle grain boundary can be a possible explanation for the difference in the graphite rotation angles. A low-angle grain boundary is composed of an array of dislocations and the tilt angle over the boundary α (in radian) is associated with the spacing of the dislocations by

$$P_D = b/\alpha, \tag{4}$$

where b is the Burgers vector and P_D is the dislocation spacing [26]. Based on the assumption that the boundary for the superlattice region with varying periodicities is a low-angle grain boundary, we have worked out the misorientation angle α from Eq. (4) along both boundaries (on the left and on the right); the misorientation angle was also found by the difference in the rotation angles of the superlattices on the two sides of the boundary (Fig. 9) assuming

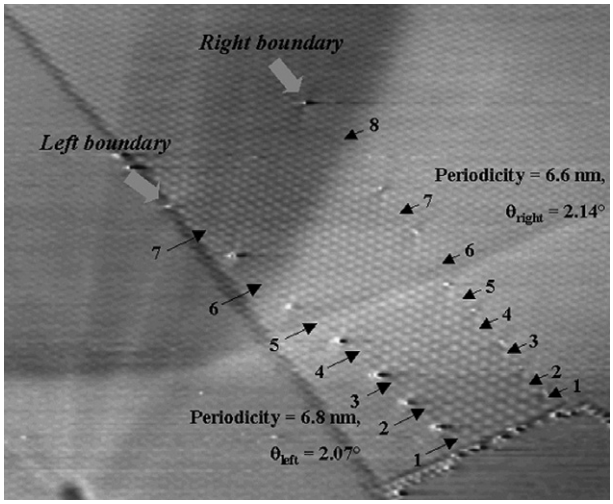

Fig. 9. 380 nm × 462 nm, $I_t = 0.5$ nA, $V_s = 206$ mV, about the same area as Fig. 5. Measurements of misorientation angle α are taken along the left and right boundaries. The misorientation angle α is worked out by two ways: firstly from the spacing of the protrusions along the boundary. The spacing of the protrusions PD can be found from the STM image, and the magnitude of the Burgers vector b is chosen to be the lattice constant of the graphite which is 0.246 nm as this value gives the most closely matched results, thus the misorientation angle can be found by Eq. (4); secondly from the periodicities of the superlattices. The rotation angle of a graphite sheet can be found from the superlattice periodicity by Eq. (3). The superlattice regions outside the boundaries are of constant periodicities, and the one on the left is of 6.8 nm (rotation angle (left = 2.07°)) while the one on the right is of 6.6 nm (rotation angle (right = 2.14°)). The misorientation angle therefore can be found by the difference between the rotation angles of the superlattices on the two sides of the boundary. The results of the measurements along the left boundary and the right boundary are shown in Tables 1a and 1b respectively. The positions where the measurements are taken are marked by the arrows and numbered; they are all midway between the protrusions.

Table 1a
The measurement results of the misorientation angle α along the right boundary of the region with non-constant superlattice periodicity by two different means (using Eqs. (3) and (4))

n	P_D (nm)	$\alpha_1 = b/P_D$ (express in degree below)	P_S (nm)	θ_n (degree)	$\alpha_2 = \theta_{right} - \theta_n$ (degree)
1	20.8	0.678	9.613	1.466	0.669
2	23.0	0.613	9.314	1.513	0.622
3	27.8	0.507	8.856	1.592	0.544
4	31.9	0.442	8.388	1.681	0.455
5	28.6	0.493	8.138	1.732	0.404
6	45.6	0.309	7.936	1.776	0.360
7	43.1	0.327	7.517	1.875	0.261
8	86.0	0.164	7.125	1.978	0.157

The notation n denotes the location of the measurement which is marked in Fig. 9, P_D is the spacing of the dislocations at the position n, b is the Burgers vector with the value of 0.246 nm, P_S is the periodicity of the superlattice, and θ_n is the rotation angle corresponding to the superlattice periodicity. The value of the constant periodicity of the superlattice on the right of the boundary θ_{right} is indicated in Fig. 9.

Table 1b
The measurement results of the misorientation angle α along the left boundary

n	P_D (nm)	$\alpha_1 = b/P_D$ (express in degree below)	P_S (nm)	θ_n (degree)	$\alpha_2 = \theta_{left} - \theta_n$ (degree)
1	25.1	0.562	9.613	1.466	0.607
2	29.4	0.479	9.200	1.532	0.541
3	33.3	0.423	8.650	1.630	0.443
4	38.7	0.364	8.133	1.733	0.340
5	45.1	0.313	7.855	1.795	0.278
6	56.9	0.248	7.571	1.862	0.211
7	64.2	0.220	7.375	1.911	0.162

The value of the constant periodicity of the superlattice on the left of the boundary θ_{left} is indicated in Fig. 9.

that the superlattices are due to a Moiré rotation. The results are listed in Tables 1a and 1b, and they are plotted in Fig. 10a and b. The value of the Burgers vector b is chosen to be one lattice constant of graphite (0.246 nm) as the results match most closely with this value. It is shown that the misorientation angles calculated by the two different means are rather close to each other and they follow the same trend: the angle decreases as we go along from the bottom part of the superlattice with varying periodicity to the upper part. Such agreement strongly suggests that the boundaries for this superlattice with varying periodicity are low-angle grain boundaries, and the Burgers vector for the boundaries is one lattice constant. The tilt induced by each dislocation is of the order 0.1°, making this an extremely low-angle grain boundary.

The tilt boundary on graphite was described briefly before [27] and studied from the theoretical point of view [28,29]. Daulan et al. [30] and Simonis et al. [31] reported their STM observation of grain boundaries in graphite with the constant tilt angles of 13° and 39° respectively. Tilt boundaries with angles of 19°, 8°, 6.5° were observed under the STM before as well [32]. However low-angle grain boundaries in graphite observed under STM were not well studied before. The protrusions on the boundaries (i.e. the dislocation points) have corrugations which are larger than that of the superlattice. In order to study this phenomenon, a model, based on the original structure proposed by Kittel for low-angle grain boundary with square lattices [26], is constructed with hexagonal lattices to replicate the surface structure along the low-angle grain boundary on a graphite layer. Since the above result shows that the value of the

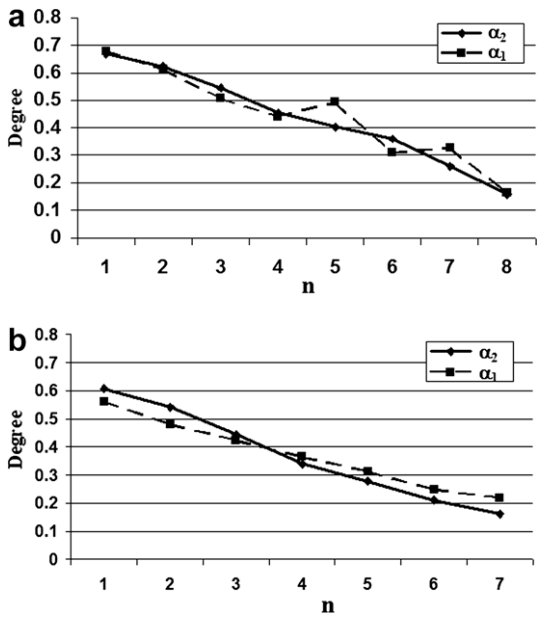

Fig. 10. (a) Plotting of the results in Table 1a for comparing the misorientation angles α found by the two different ways along the right boundary of the superlattice with varying periodicity. (b) Plotting of the results in Table 1b for comparing the misorientation angles α found by the two different ways along the left boundary of the superlattice with varying periodicity.

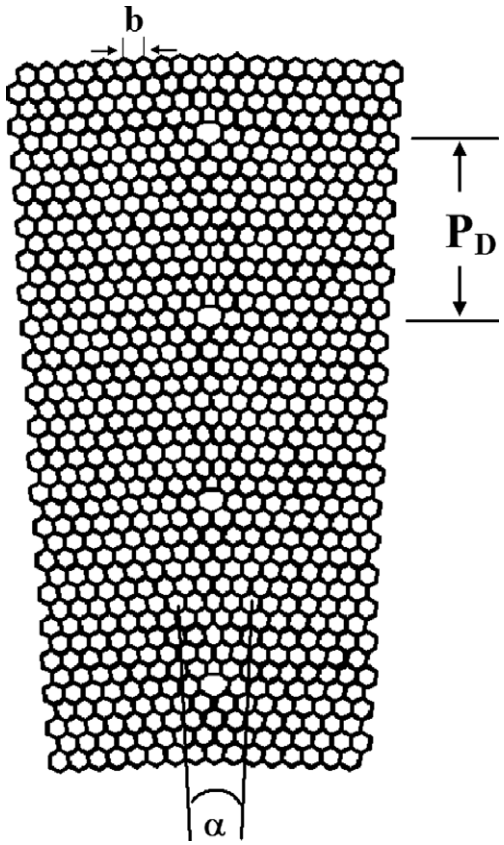

Fig. 11. A simplistic model of a low-angle grain boundary consisting of the hexagonal lattices of graphite. There is a misorientation angle α between the left lattice and the right lattice, which are separated by an array of dislocations (in the form of pentagon–heptagon pairs) in the middle. The spacing of the dislocation P_D and the magnitude of the Burgers vector b are related to the misorientation angle by Eq. (7). This model is just to crudely illustrate the idea of a low-angle grain boundary on a graphite surface, and it is not meant to truly represent the boundaries of the superlattice with non-constant periodicity in Fig. 5 because this model does not take into account the varying misorientation angle along the boundary.

lattice constant gives the best matched results, the magnitude of the Burgers vector in the model is assigned to be 0.246 nm. This value of a lattice constant (0.246 nm) was also used by Garbarz et al. for the Burgers vector in constructing their model of honeycomb twist sub-boundaries on graphite [3]. Soto [33] found that a vacancy in graphite will create a charge enhancement in the atoms directly surrounding it. We therefore kept the number of vacancies as small as possible and minimized the number of bonds affected in the model. In Fig. 11, there are two hexagonal lattices with a misorientation angle α between them along the array of dislocation in the middle. This is obviously a rather naive qualitative model which by no means can truly represent the low-angle grain boundary with varying dislocation spacings as we observed by STM, as the misorientation angle α is constant in this model. We exhibit this model simply for the purpose of roughly illustrating a low-angle grain boundary in a hexagonal lattice. This model is similar to the atomic model of the grain boundary of Simonis et al. (Fig. 3 in Ref. [31]) which they built for the grain boundary with a tilt angle of 39° in that both models have an array of dislocations at the boundary. In our model, the dislocations are in the form of an array of pentagon–heptagon pairs, similar to the pentagon–heptagon dislocation sites in the model of Simonis et al. but with opposite direction; the separation between the dislocations is just one row of hexagons whereas there are ten rows in our model. We believe the pentagon–heptagon dislocation sites enhance the local density of states which lead to the increased charge density at the dislocations, consequently the dislocation network along the low-angle grain boundary appears as an array of protrusions.

Now, as the superlattice boundaries are identified as low-angle grain boundaries with varying tilt angles and modelled with hexagonal lattices and pentagon–heptagon dislocations, further explanation can be provided to the superlattices observed in Fig. 5a. The situation here is quite complicated because the regions on both sides of the superlattice region with varying periodicity show the conventional superlttices. Fig. 5b provides a schematic model delineating the relationship between these three areas. Low-angle grain boundaries with varying tilt angles exist between regions A and B (LAGB I) and between regions B and C (LAGB II) on the top graphite layer. As discussed above, the low-angle grain boundaries here are acting like media through which the Moiré rotation angles will be altered from one side to the other. Since the tilt angles vary along the boundaries, the alterations of the Moiré rotation angles are different from one ends of the boundaries to the others. As such, the uniform atomic lattice orientation in region A is changed by LAGB I into a range of atomic lattice orientations in region B, resulting in a superlattice with varying periodicity in region B. From region B to C, LAGB II happens to convert the range of the atomic lattice orientations in region B back to a uniform atomic lattice orientation in region C. In order for this to occur, the directions of the pentagon–heptagon dislocations of LAGB I and LAGB II must be opposite to each other so that the alternations of atomic lattice orientations at LAGB II are the other way around as opposed to those at LAGB I. This explains why there are conventional superlattices outside the superlattice region with varying periodicity.

Although atomic resolution images on the array of protrusions were not obtained due to the sharpness of the tip, we believe that our interpretation of the superlattice boundary from the perspective of a low-angle grain boundary is scientifically sound because the tilt angles measured from the spacing of the protrusions and the tilt angles measured from the superlattice periodicities agree with each other very well (as shown in Fig. 10a and b), strongly indicating that the superlattice boundary is indeed a low-angle grain boundary.

Based on the idea that the tilt angle of the low-angle grain boundary is the origin of the difference in the super-

Table 2a
The periodicities of the dislocations P_D and the superlattices on the two sides of the right boundary (P_1 for the superlattice periodicity on the right of the boundary while P_2 for the superlattice periodicity on the left of it) in Fig. 9 and their corresponding reciprocals

n	P_D (nm)	P_1 (nm)	P_2 (nm)	$1/P_D$	$1/P_1$	$1/P_2$	$1/P_1 - 1/P_2$
1	20.8	6.6	9.613	0.04808	0.1515	0.1040	0.04749
2	23	6.6	9.314	0.04348	0.1515	0.1074	0.04415
3	27.8	6.6	8.856	0.03597	0.1515	0.1129	0.03860
4	31.9	6.6	8.388	0.03135	0.1515	0.1192	0.03230
5	28.6	6.6	8.138	0.03497	0.1515	0.1229	0.02864
6	45.6	6.6	7.936	0.02193	0.1515	0.1260	0.02551
7	43.1	6.6	7.517	0.02320	0.1515	0.1330	0.01848
8	86	6.6	7.125	0.01163	0.1515	0.1404	0.01116

Table 2b
The periodicities of the dislocations and the superlattices on the two sides of the left boundary (P_1 for the superlattice periodicity on the left of the boundary while P_2 for the superlattice periodicity on the right of it) in Fig. 9 and their corresponding reciprocals

n	P_D (nm)	P_1 (nm)	P_2 (nm)	$1/P_D$	$1/P_1$	$1/P_2$	$1/P_1 - 1/P_2$
1	25.1	6.8	9.613	0.03984	0.14706	0.1040	0.04303
2	29.4	6.8	9.2	0.03401	0.14706	0.1087	0.03836
3	33.3	6.8	8.65	0.03003	0.14706	0.1156	0.03145
4	38.7	6.8	8.133	0.02584	0.14706	0.1230	0.02410
5	45.1	6.8	7.855	0.02217	0.14706	0.1273	0.01975
6	56.9	6.8	7.571	0.01758	0.14706	0.1321	0.01498
7	64.2	6.8	7.375	0.01558	0.14706	0.1356	0.01147

lattice periodicities across the boundary, a further study is performed on the relationship between the periodicities of the boundary dislocations and the superlattices. Eq. (3) can be rewritten in this form:

$$P_S = d/[2 \times \sin(\theta/2)] \approx d/\theta,$$

where the rotation angle of the superlattice θ is small (e.g. less than 5°), and thus

$$\theta \approx d/P_S, \tag{5}$$

where d is the lattice constant and P_S is the superlattice periodicity. It is our assumption that the tilt angle of the boundary α is equal to the difference between the rotation angles of the superlattices on the two sides of the boundary (θ_1, θ_2 are the rotation angles and P_1, P_2 are the periodicities of the superlattices on the two sides of the boundary), therefore

$$\alpha = \theta_1 - \theta_2 \approx d/P_1 - d/P_2, \tag{6}$$

while Eq. (4) also gives the tilt angle

$$\alpha = b/P_D. \tag{7}$$

Hence Eq. (6) can be related to Eq. (7) and this gives

$$b/P_D \approx d/P_1 - d/P_2$$

and since b and d have the same numerical value, we arrive at this equation

$$1/P_D \approx 1/P_1 - 1/P_2, \tag{8}$$

which means the reciprocal of the boundary dislocation periodicity is approximately equal to the difference between the reciprocals of the periodicities of the superlattice on each side of the low-angle grain boundary. In order to justify this equation, the data in Tables 1a and 1b are used to find the reciprocal periodicities which are presented in Tables 2a and 2b. The results are plotted in Fig. 12a and b, and it is shown that the $1/P_D$ values are very close to

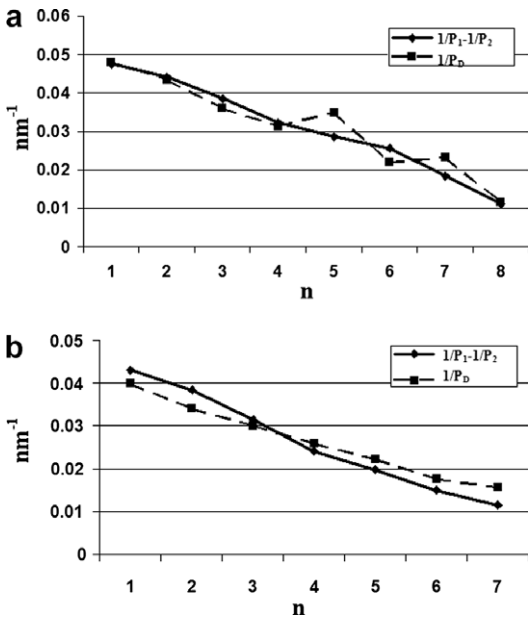

Fig. 12. (a) Plotting of the results in Table 2a for comparing $1/P_D$ and $1/P_1 - 1/P_2$ along the right boundary of the superlattice with varying periodicity to verify the relationship in Eq. (8). (b) Plotting of the results in Table 2b for comparing $1/P_D$ and $1/P_1 - 1/P_2$ along the left boundary of the superlattice with varying periodicity.

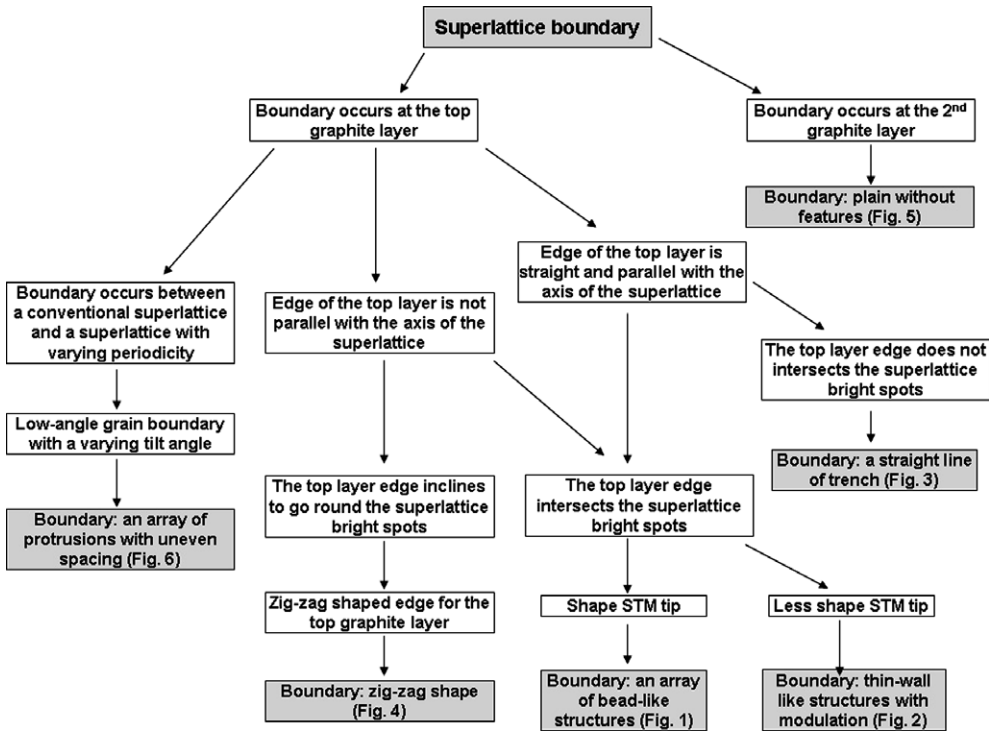

Fig. 13. Flow chart illustrating our explanation on the formation and origin of superlattice boundaries.

the $1/P_1 - 1/P_2$ values and they follow the same trend. This suggests that Eq. (8) can be interpreted as the boundary dislocations being the cause of the difference in the superlattice periodicities across the boundary, which is not surprising as the dislocations induce the shift of the graphite lattice structure which in turn brings along the change of the superlattice rotation angle. Introducing terms for dislocation frequency F_D and superlattice frequency F_P, which are reciprocal to their corresponding periodicities, then Eq. (8) becomes

$$F_D \approx F_{P_1} - F_{P_2}. \tag{9}$$

This equation describes the situation that the superlattice, which is two dimensional, has its frequency adjusted by the frequency of the dislocation array which is one dimensional.

Our experimental data, together with the Eqs. (8) and (9) derived give a precise physical description to the correlation between the graphite superlattice with varying periodicity and the low-angle grain boundary. Our work on the low-angle grain boundary delivers an important scientific information because firstly, superlattices with varying periodicity have only been reported for a few times without too much discussion (refer to [7 and 10]), and it is of much interest to understand their origins; secondly, the low-angle grain boundaries observed here have extremely small tilt angles, of the order of 0.1°. Such low tilt angles have rarely been seen by any means. The phenomenon that the low-angle grain boundaries have their varying tilt angles manifested by the variation of the periodicity of the superlattice in its own right is not explored before.

5. Conclusion

In this work, we have reported our observation on several types of superlattice boundary. Analysis is given from an energetic point of view and an explanation for the formation of the boundaries is provided. The relationship between the low-angle grain boundary and the superlattice with varying periodicity is investigated and an equation relating the periodicity of the boundary dislocations to the periodicities of the superlattices across the boundary is derived. Fig. 13 summarizes our discussion on the formation and origin of superlattice boundaries and provides an overall picture for their occurrences. Our analysis has successfully explained the formation of several different types of superlattice boundaries qualitatively. However, theoretical work is needed to further justify our theory and elucidate some properties of superlattice boundaries, for example, what determines the ratio between the corrugations of a bead-like boundary and its corresponding superlattice (in our case, the ratio is $0.26/0.17 = 1.53$) and how much energy can a system lower by having a zig-zag shaped boundary. Future work also involves atomic resolution imaging on a low-angle grain boundary with a varying tilt angle which separates a conventional superlattice and a superlattice with varying periodicity so as to provide additional support to the pentagon–heptagon dislocation model proposed in this paper. The manifestation of an

extremely low-angle grain boundary (of the order of 0.1°) as a superlattice with varying periodicity from 7.1 to 9.6 nm suggests that Moiré superlattices can be a tool for observing minute surface deformations as we have proposed previously [34].

Acknowledgment

The authors are grateful for the research funding by European Union IST project "QIDPPF – ROSES".

References

[1] Z.Y. Rong, P. Kuiper, Phys. Rev. B 48 (1993) 17427.
[2] M. Kuwabara, D.R. Clarke, D.A. Smith, Appl. Phys. Lett. 56 (1990) 2396.
[3] J. Garbarz, E. Lacaze, G. Faivre, S. Gauthier, M. Schott, Philos. Mag. A 65 (1992) 853.
[4] J. Xhie, K. Sattler, M. Ge, N. Venkateswaran, Phys. Rev. B 47 (1993) 15835.
[5] Z.Y. Rong, Phys. Rev. B 50 (1994) 1839.
[6] V.J. Cee, D.L. Patrick, T.P. Beebe Jr., Surf. Sci. 329 (1995) 141.
[7] T.M. Bernhardt, B. Kaiser, K. Rademann, Surf. Sci. 408 (1998) 86.
[8] J. Osing, I.V. Shvets, Surf. Sci. 417 (1998) 145.
[9] P.J. Ouseph, Phys. Rev. B 53 (1998) 9610.
[10] B. Feddes, I.I. Kravchenko, L.E. Seiberling, Scanning 20 (1998) 376.
[11] K. Miyake, K. Akutsu, T. Yamada, K. Hata, R. Morita, M. Yamashita, H. Shigekawa, Ultramicroscopy 73 (1998) 185.
[12] H. Beyer, M. Muller, Th. Schimmel, Appl. Phys. A 68 (1999) 163.
[13] P.J. Ouseph, Appl. Surf. Sci. 165 (2000) 38.
[14] K. Kobayashi, Phys. Rev. B 53 (1996) 11091.
[15] H.L. Sun, Q.T. Shen, J.F. Jia, Q.Z. Zhang, Q.K. Xue, Surf. Sci. 542 (2003) 94.
[16] W.T. Pong, C. Durkan, in: Proceedings of the 5th International Conference 7th Annual General Meeting of the European Society for Precision Engineering and Nanotechnology, Montpellier, France, 2005, vol. 1, p. 241.
[17] easyScan system by Nanosurf AG, Switzerland.
[18] J.E. Buckley, J.L. Wragg, H.W. White, J. Vac. Sci. Technol. B 9 (1991) 1079.
[19] J.-C. Charlier, J.-P. Michenaud, P. Lambin, Phys. Rev. B 46 (1992) 4540.
[20] H. Chang, A.J. Bard, Langmuir 7 (1991) 1143.
[21] C.R. Clemmer, T.P. Beebe Jr., Science 251 (1991) 640.
[22] Y. Gan, W. Chu, L. Qiao, Surf. Sci. 539 (2003) 120.
[23] G. Dai, T. Xie, H. Cheng, H. Ye, J. Mater. Sci. Technol. 19 (2003) 246.
[24] R. Hentschke, B. Schurmann, J. Rabe, J. Chem. Phys. 96 (1992) 6213.
[25] W.T. Pong, C. Durkan, Jpn. J. Appl. Phys. 44 (7B) (2005) 5365.
[26] C. Kittel, Introduction to Solid State Physics, sixth ed., John Wiley & Sons, New York, 1986 (Chapter 20, p. 567).
[27] S. Amelinckx, P. Delavignette, M. Heerschap, in: P.L. Walker Jr. (Ed.), Chemistry and Physics of Carbon, vol. 1, M. Dekker Inc., New York, 1965, p. 41.
[28] G.L. Bleris, G. Nouet, S. Hagege, P. Delavignette, Acta Cryst. A 38 (1982) 550.
[29] H. Grimmer, D.H. Warrington, Acta Cryst. A 43 (1987) 232.
[30] C. Daulan, A. Derré, S. Flandrois, J.C. Roux, H. Saadaoui, J. Phys. I France 5 (1995) 1111.
[31] P. Simonis, C. Goffaux, P.A. Thiry, L.P. Biro, Ph. Lambin, V. Meunier, Surf. Sci. 511 (2002) 319.
[32] T.R. Albrecht, H.A. Mizes, J. Nogami, S. Park, C.F. Quate, Appl. Phys. Lett. 52 (1988) 362.
[33] M.R. Soto, J. Microscopy 152 (1988) 779.
[34] W.T. Pong, C. Durkan, J. Phys. D 38 (2005) 329.